Demonstrator Testbed for Effective Precoding in MEO Multibeam Satellites

Jorge L. González-Rios*, Liz Martínez Marrero, Juan Duncan*, Luis M. Garcés-Socarrás,
Raudel Cuiman Marquez, Juan Andres Vásquez Peralvo, Jevgenij Krivochiza, Symeon Chatzinotas,
Björn Ottersten
SnT, University of Luxembourg, Luxembourg
*Corresponding authors: {jorge.gonzalez,juan.duncan}@uni.lu

***Abstract*—The use of communication satellites in medium Earth orbit (MEO) is foreseen to provide quasi-global broadband Internet connectivity in the coming networking ecosystems. Multi-user multiple-input single-output (MU-MISO) digital signal processing techniques, such as precoding, emerge as appealing technological enablers in the forward link of multi-beam satellite systems operating in full frequency reuse (FFR). However, the orbit dynamics of MEO satellites pose additional challenges that must be carefully evaluated and addressed. This work presents the design of an in-lab testbed based on software-defined radio (SDR) platforms and the corresponding adaptations required for efficient precoding in a MEO scenario. The setup incorporates a precise orbit model and the radiation pattern of a custom-designed direct radiating array (DRA). We analyze the main impairments affecting precoding performance, including Doppler shifts and payload phase noise, and propose a synchronization loop to mitigate these effects. Preliminary experimental results validate the feasibility and effectiveness of the proposed solution.**

***Index Terms*—precoding, medium Earth orbit, multi-beam satellite, in-lab testbed, SDR, direct radiating array**

I. Introduction

The use of communication satellites in medium Earth orbit (MEO) for quasi-global broadband Internet connectivity is expected to be instrumental within the sixth generation (6G) networking ecosystem [1]. The growing demand for broadband and trunking traffic has prompted the pursuit of approaches that can supply additional spectrum to next-generation systems. MEO satellites offer lower latency than geostationary orbit (GEO) ones, with better scalability while maintaining link reliability [2].

Multi-user multiple-input single-output (MU-MISO) digital signal processing techniques, such as precoding [3]–[5], emerge as key enablers in the forward (FWD) link of multi-beam satellite systems operating in full frequency reuse (FFR). Precoding will empower future MEO missions by providing flexibility and capacity, while shifting complexity toward the ground segment, where gateways (GWs) can handle a higher processing burden.

This work has been supported by the European Space Agency under the project number 4000122451/18/NL/NR "Live Satellite Precoding Demonstration - CCN: MEO case (LiveSatPreDem)" (Opinions, interpretations, recommendations, and conclusions presented in this paper are those of the authors and are not necessarily endorsed by the European Space Agency). This work has been funded in part by the Luxembourg National Research Fund (FNR), grant reference INTER/MOBILITY/2023/IS/18014377/MCR.

To evaluate the feasibility of precoding in communication satellites, our group initiated the LiveSatPredem (Live Satellite Precoding Demonstration) project in 2018. Through live demonstrations and laboratory-controlled end-to-end emulations, this activity focuses on precoding for the forward link of multi-beam satellite systems in FFR [5]–[7]. Nevertheless, precoding has been more studied in GEO than in MEO systems [6], [8]. This trend is changing with the growing interest in MEO, and recent works have explored precoding in this orbit [9]–[11], although most still rely exclusively on simulations.

In this context, this work presents the design of an in-lab testbed based on software-defined radio (SDR) with adaptations for MEO precoding. The main contributions are: (i) development of a realistic MEO multibeam scenario integrating precise orbital dynamics and the radiation pattern of a custom-designed direct radiating array (DRA); (ii) design and implementation of a phase compensation loop to mitigate fast differential phase variations, particularly those induced by uplink Doppler shifts and payload phase noise; (iii) upgrade of an existing SDR-based MIMO satellite channel emulator to reproduce MEO-specific impairments; and (iv) experimental assessment of the impact of individual and combined impairments on precoding performance, demonstrating the effectiveness of the mitigation approach.

II. System Model

We consider a MEO satellite equipped with a DRA generating N beams serving $K \leq N$ single-antenna User Terminals (UTs). We collect in $\mathbf{h}_k \in \mathbb{C}^{N\times 1}$ the complex coefficients of the frequency-flat slow fading channels between the beams generated at the GW and the k-th UT. At a given symbol period, independent data symbols $\{s_k\}_{k=1}^{K}$ are transmitted to the UTs, where s_k denotes the symbol intended for the k-th user.

Under these assumptions, the received vector with the symbol-sampled complex baseband signals of all K UTs can be modeled as

$$\mathbf{r} = \mathbf{H}\mathbf{W}\mathbf{s} + \mathbf{z}, \tag{1}$$

where $\mathbf{H} = [\mathbf{h}_1 \cdots \mathbf{h}_K]^{\mathrm{T}}$ denotes the $K \times N$ channel matrix, $\mathbf{W}$ is the $N \times K$ precoding matrix, $\mathbf{s} = [s_1 \cdots s_K]^{\mathrm{T}}$ the $K \times 1$ vector of intended symbols, and $\mathbf{z}$ the independent complex zero-mean AWGN at the UT receivers.

The channel matrix can be expressed as

$$\mathbf{H}(t) = \begin{bmatrix} |h_{11}(t)|e^{j\psi_{11}(t)} & \cdots & |h_{1N}(t)|e^{j\psi_{1N}(t)} \\ |h_{21}(t)|e^{j\psi_{21}(t)} & \cdots & |h_{2N}(t)|e^{j\psi_{2N}(t)} \\ \vdots & \vdots & \vdots \\ |h_{K1}(t)|e^{j\psi_{K1}(t)} & \cdots & |h_{KN}(t)|e^{j\psi_{KN}(t)} \end{bmatrix}, \quad (2)$$

where h_{kj} denotes the channel coefficient between the k-th UT and the j-th beam, with $|h_{k,j}|$ and $\psi_{k,j}$ its magnitude and phase. The time-varying terms $|h_{kj}(t)|$ represent the magnitude of the channel gain, which varies with the changing elevation angle between satellite and UT.

A time-varying diagonal matrix $\mathbf{\Gamma}(t) \triangleq \text{diag}(e^{j\epsilon_1(t)}, e^{j\epsilon_2(t)}, ..., e^{j\epsilon_K(t)})$ accounts for Doppler-induced phase variations. The complete channel matrix becomes

$$\mathbf{H}_{\text{MEO}}(t) = \mathbf{\Gamma}(t)\mathbf{H}(t). \quad (3)$$

The time-varying gain and phase variations in the channel matrix are addressed by the precoding design considered in this paper. These impairments depend on the satellite orbit and the UT ground locations.

A. Satellite Orbit Model

The forward channel performance depends on time-varying propagation effects from the satellite's orbital motion. We obtained the parameters using MATLAB for a MEO satellite, although the same method applies to other NGSO orbits such as LEO. The input is the TLE data of the O3B FM5 satellite from Celestrak[1] and the on-board antenna described next. We considered a GW in Dakar and four nearby UTs. Their coordinates and the carrier frequencies are given in Tables I and II.

TABLE I
GROUND STATION (GS) COORDINATES

GS	GW	UT0	UT1	UT2	UT3
Latitude	14.74	12.94	12.94	14.74	14.74
Longitude	-17.49	-19.35	-17.49	-19.35	-17.49

TABLE II
FREQUENCY PLAN

Beam	Uplink0	Uplink1	Uplink2	Uplink3	Downlink
Freq. (GHz)	47.2	47.7	48.2	48.7	20.0

B. Antenna Design

A DRA was selected for a MEO link in the 17.7–20.2 GHz band to generate a ≈150,000 km^2 spot beam with right- and left-hand circular polarization, 2° beamwidth, and a 50 × 50 element configuration. The elements are fed through a microstrip network with 90° phase shift, coupled via a square aperture to excite orthogonal modes for circular polarization, and optimized with foam layers for impedance bandwidth and axial ratio. CST simulations confirmed compliance with reflection coefficient, axial ratio, and gain requirements [12].

The array, with $\lambda_0/2$ spacing and overall size $25\lambda_0 \times 25\lambda_0$, was analyzed using the array factor formulation, combining element pattern and geometry to obtain gain and directivity. The resulting pattern (Fig. 1) shows cross-polarization about 20 dB below the co-polar maximum, 2° beamwidth at boresight, and similar principal cuts, ensuring the pencil beam shape required for beam steering.

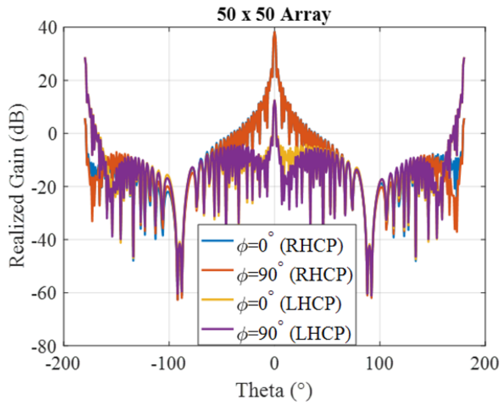

Fig. 1. Co-polar and cross-polar full array radiation pattern.

C. Scenario Definition

Figures 2 to 4 depicts the calculated orbital and channel parameters for the selected scenario, considering 20 minutes around the zenith. In the case of the Doppler shift (c.f. Fig. 2), in the experiments we apply a scaled version of the original values, considering that the GW can estimate the Doppler shift with a precision of +/-1 kKz [13] and apply a precompensation (we do not assume perfect compensation though). The carrier-to-interference-ratio (C/I) in Fig. 4 is calculated from the 16 (4×4) complex channel coefficients and provided here as a compact representation of the channel, although the testbed uses the full time-varying matrix as an input. The ripple in the C/I curves arises from the satellite's movement, which is not perfectly elliptical and is affected by the actual orbital perturbations, combined with the effects of the changes on the pointing angle on the DRA radiation pattern.

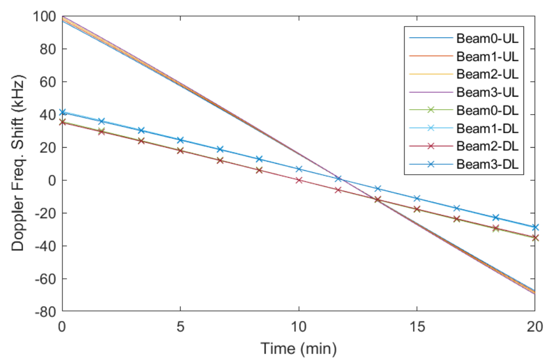

Fig. 2. Doppler shift for each beam in uplink (UL) and downlink (DL).

[1]https://celestrak.org/

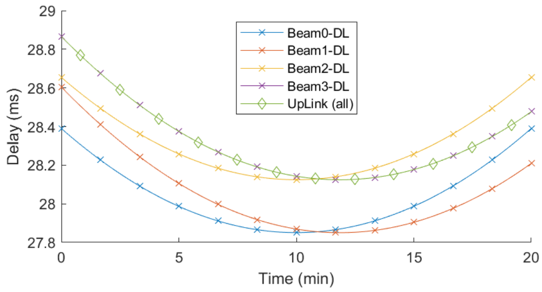

Fig. 3. Delay for each beam in uplink and downlink (DL).

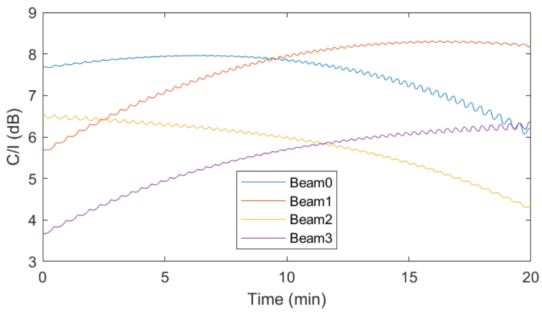

Fig. 4. Nominal carrier-to-interference ratio (C/I)

Moreover, Fig. 5 shows the power spectral density of the phase noise applied to each beam (fully uncorrelated), following the model described in [14].

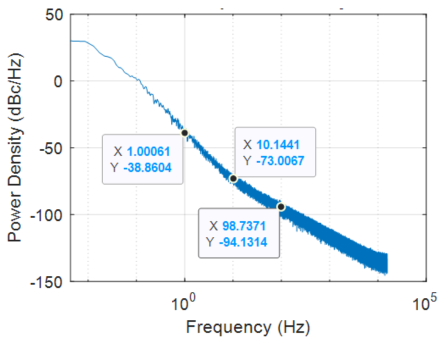

Fig. 5. Phase noise power spectral density for each beam.

III. Precoding with Phase Compensation Design

Conventional precoding assumes perfect beam phase control, but practical systems suffer from fast phase variations introduced by the phase noise of local oscillators (LOs) and Doppler shift. It was formally demonstrated in [15] that the performance of precoding techniques is only affected by the phase errors in the uplink channel. That is, independent phase rotations per beam, such as the differential Doppler shift in the uplink due to frequency-division multiplexing (FDM), and the phase noise of the transponder's independent LOs. These effects cause rapid differential phase errors that the conventional, slow-updating precoding loop cannot fully compensate. To address this, we implement a second-order, fast-response compensation loop operating in a sample-based mode, enabling more effective mitigation than the symbol/frame-based updates used in standard precoding. The solution is represented in Fig. 6, where only phase and frequency parameters are considered. In the figure, the n-th beam is represented by its carrier frequency f_n^{U}, and the phase noise introduced in the uplink process is represented as ϕ_n^{U}. The Channel block includes the phase rotations due to the Doppler effect as explained in (3). The CSI estimated by the k-th UT has the form $[\hat{\psi}_{k,1}\ \hat{\psi}_{k,2}\ \cdots\ \hat{\psi}_{k,N}]$, with $\hat{\psi}_{k,j} = \psi_{k,j} - \psi_{k,k}$. The term $\psi_{k,j}$ includes the phase errors mentioned before. This CSI is obtained through a conventional data-aided algorithm using non-precoded pilots.

The differential phase error is compensated at the GW by modifying the frequency offset applied to the numerically controlled oscillator (NCO) used in the digital up-conversion. Unlike conventional precoding implementations, where the differential phase compensation is updated for several symbols or frames, the phase error is compensated for each sample in our design. To this end, a compensation phase ϕ_n is generated by a time-invariant linear controller using the interpolated version of the received CSI phase as input.

IV. Hardware Test-Bed Implementation

For the experimental validation, we employ the in-house developed MIMO end-to-end satellite emulator based on software-defined radio (SDR) platforms, shown in Fig. 7. The proposed architecture consists of a multichannel GW with precoding capabilities, a MIMO satellite channel emulator (ChEm), a set of independent UTs, and a return-link emulator.

Figure III shows a summary of the parameters used in the experiments.

TABLE III
Parameters of the Precoding Experiment

Parameter	Value
Protocol	DVB-S2X Super Frame Format 2
Modulation	QPSK
Baud Rate	3.1 MBaud
Oversampling factor	4
Pulse Shaping Filter	Square Root Raised Cosine (SRRC)
Rolloff-factor (α)	0.20 (20%)
Pilot Length	36 symbols (as defined in standard)
Interpilot Length	956 symbols
CSI Averaging Time	100 pilots (95600 symbols or 30.84 ms)
Phase Controller Update time	100 pilots (same as CSI/Precoding)
Phase Controller Acting Time	One symbol time (4 sample periods)
Phase Controller PLL type	Type-2 PLL

In general terms, the demonstrator can be described as follows. The GW subsystem generates the data packets according to the DVB-S2X standard, using Superframe Format II structure, and applies the selected precoding method. The ChEm replicates the whole forward link chain, from the intermediate frequency (IF) input of the gateway block up-converter (BUC), toward the low-noise block down-converter (LNB) IF output at the user terminal. It emulates the impairments present in the GW, the payload, the downlink channel, and the UTs. The

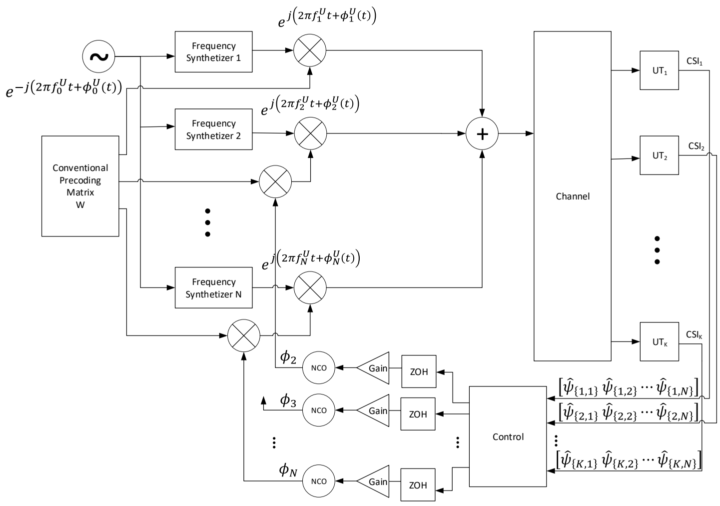

Fig. 6. Differential phase-error compensation loop.

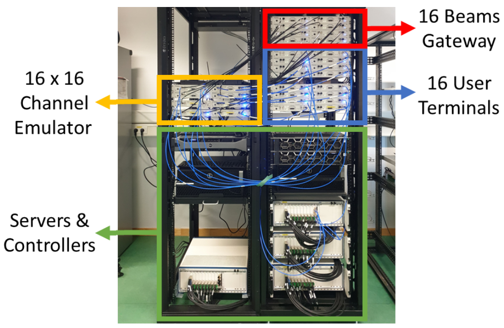

Fig. 7. SDR-based MIMO end-to-end satellite emulator.

UT subsystems implement the synchronization and decoding features in the DVB-S2X-compliant receivers and perform the CSI estimation. Finally, the return-link emulator allows each UT to send its estimated CSI to the GW.

The GW, ChEm, and UT subsystems are being implemented using a set of SDR platforms, specifically the USRP-2944R from National Instruments. The physical interfaces of the channel emulator with the gateway and the user terminals are provided by the interconnection of the 50-Ω ports of the SDRs, employing IF modulated signals. The SDR platforms in the GW and the channel emulator are synchronized with the same frequency and clock references. This eliminates any timing misalignment and additional phase noise due to USRPs' LOs, allowing precise control of the time, frequency, and phase impairments according to the implemented models.

All the components of the system have been successfully tested considering a GEO satellite scenario [6], [16]. This includes the use of implementations of the GW and UTs subsystems in the precoding validation over a live GEO link [6]. The channel emulator is upgraded with the inclusion of the time-varying channel matrix in the downlink, the Doppler frequency shifts, and the delays, as shown in Fig. 8. These effects are obtained from the orbit and antenna models, presented in Section II. Some of the new blocks have also been tested individually in other activities, namely the Doppler shift in [17], and the variable delay in [18]. The GW subsystem incorporates the implementation of the compensation technique [14].

V. RESULTS

This section presents the assessment of the MEO impairments' impact on the precoding scheme and the validation of the phase compensation technique. On top of the scenario parameters described in Section II-C, we introduced independent AWGN to each beam, with an average signal-to-noise-ratio (SNR) of 10 dB.

We first corroborated that the synchronization chain in the receivers can track the time-varying impairments. Fig. 9 depicts the signal-to-interference-plus-noise-ratio (SINR) measured by each UT when all the impairments are applied in the channel emulator and the precoding is not activated in the GW. Different effects can be observed, for instance, the time-varying gain of the channel, including the ripple provided by the realistic emulated orbit in the channel emulator. There are also noticeable perturbations around the center of the plots, corresponding to the changes of sign in the Doppler shifts. On the other hand, the pronounced variations of SINR at the beginning and end of the plots are artifacts due to the switching times for setting up the scenario in the channel emulator.

Next, we assessed the effect of each of the impairments individually on the precoding performance. We considered the baseline to be the sub-scenario where only the time-varying channel matrix and AWGN are applied, which provides an upper bound for the precoding gain in terms of SINR increment. Then we applied each of the other impairments, once at a time, in addition to the time-varying H and noise, and finally the complete scenario (all impairments together). Fig. 10 illustrates the results when precoding is activated for the baseline, with an evident improvement of the perceived

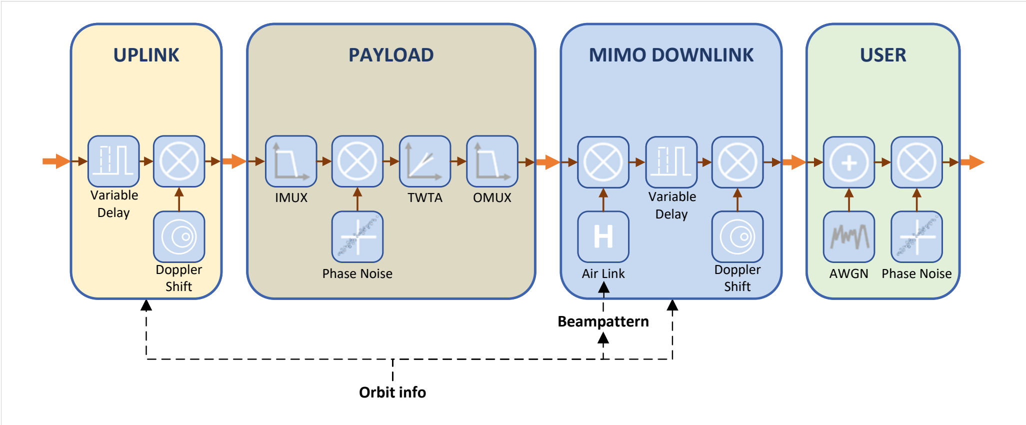

Fig. 8. Block diagram of the NGSO Channel Emulator.

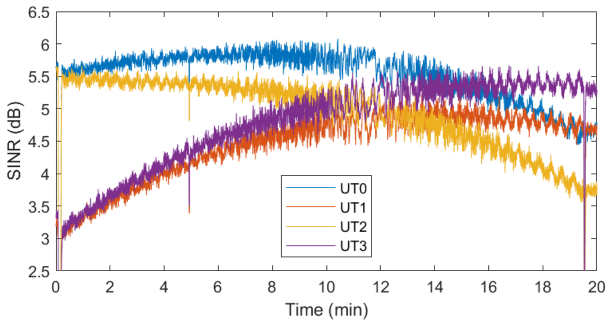

Fig. 9. Measured SINR per UT. All impairments are applied. Precoding OFF.

SINR compared to the non-precoded case. Averaging across the UTs, the SINR has an increment that varies between 1.8 and 2.6 dB during the experiment.

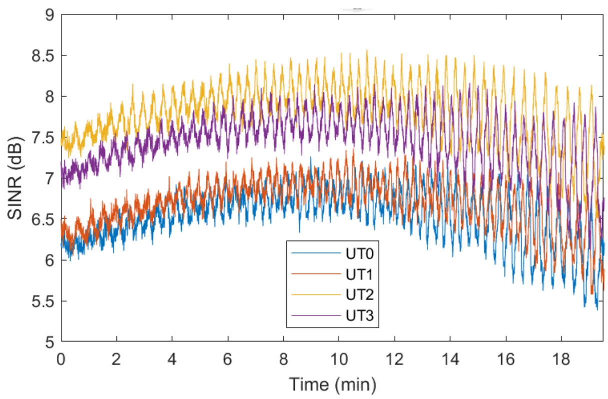

Fig. 10. Measured SINR per UT with precoding ON, only variable H and AWGN are applied (baseline).

Fig. 11 shows the measured SINR with precoding, averaged across the four UTs, for each of the tested conditions. It also includes the SINR without precoding (OFF) for comparison. The results confirm that the impairments in the downlink (different Doppler shifts and delays) and the delay in the uplink, which is the same for each of the beams, do not affect precoding. The experiment with independent phase noises in the payload shows that precoding is capable of tracking those phase variations to some extent, although its performance is not optimal because the precoding matrix is only updated at a limited rate. On the other hand, the different Doppler shifts in the uplink appear as the most critical impairment, without any precoding gain for most of the time, and an oscillatory behaviour of the SINR near the time when the frequency shifts change sign. Moreover, the joint effect of multiple non-idealities (combining all impairments) is not simply additive and significantly limits the effectiveness of precoding. In fact, the resulting SINR remains below the achievable value in the non-precoded case, dropping to as low as 1 dB (>3 dB loss). However, the precoding performance improves and achieves almost the baseline results when the satellite passage is around the zero-differential-Doppler interval. This highlights the complexity of mitigating all MEO impairments simultaneously and underscores the need for robust compensation mechanisms.

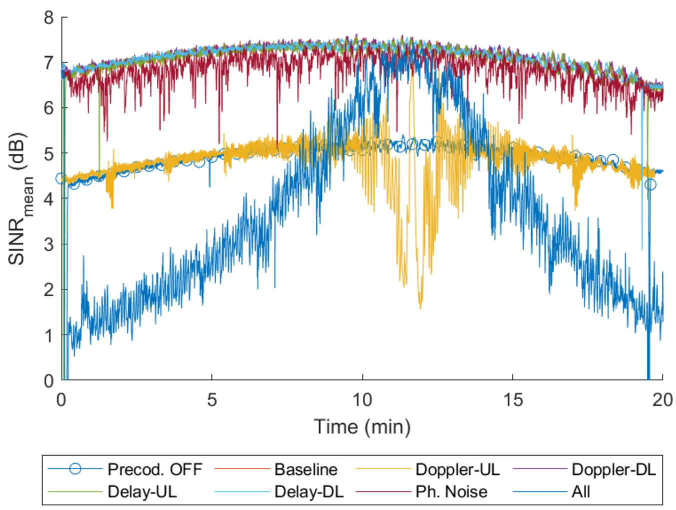

Fig. 11. Effect of the different impairments on the precoding performance. Measured SINR averaged across UTs for each tested condition.

Finally, Fig. 12 demonstrates the effectiveness of the implemented compensation technique, enabling an improvement in precoding performance for most of the satellite passage. It obtains an SINR very close to the precoding baseline scenario (i.e., what can be obtained with precoding in the absence of other impairments), with a difference of less than 0.5 dB in most of the experimentation time.

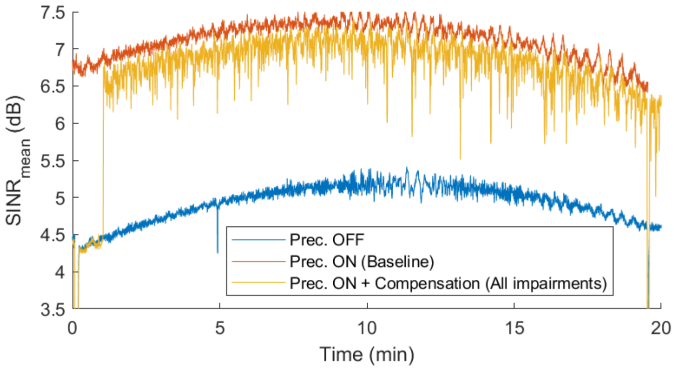

Fig. 12. Validation of the effectiveness of the phase compensation technique on the precoding performance. Measured SINR averaged across UTs for each tested condition.

Future work will investigate the optimization of the compensation mechanism to further improve its performance. We will also look into the emulation of efficient and flexible on-board beamforming techniques focusing on DRAs [19]–[22].

VI. Conclusions

This paper has presented the design and validation of an SDR-based in-lab testbed for assessing precoding performance in MEO multibeam satellite systems under realistic conditions. By incorporating accurate orbital models, antenna patterns, and key physical-layer impairments, the setup enables a comprehensive evaluation of the challenges posed by MEO dynamics. Experimental results show that while some impairments have a limited impact on precoding, uplink differential Doppler and independent payload phase noise can significantly degrade its performance. The proposed sample-based phase compensation loop effectively mitigates these effects, recovering most of the precoding gain and approaching the baseline performance with less than 0.5 dB loss.

Acknowledgment

The authors would like to thank J. Krause, J. Grotz, and S. Andrenacci from SES, Luxembourg, for their helpful advice on various practical aspects, and N. Mazzali and P.-D. Arapoglou, technical officers from ESA supervising the Livesat-CCN activity. The authors also thank the rest of Univ. of Luxembourg's team that participated in the Livesat project: J. Querol, N. Maturo, E. Lagunas, R. Palisetty, G. Eappen, H. Chaker, Z. Abdullah, W.A. Martins, and A. Haqiqtnejad.

References

[1] F. Vidal, H. Legay, G. Goussetis *et al.*, "Benchmark of MEO multibeam satellite adaptive antenna and payload architectures for broadband systems," in *10th Advanced Satellite Multimedia Systems Conference and 16th Signal Processing for Space Communications Workshop (ASMS/SPSC)*, 2020.

[2] C. I. Kourogiorgas, N. Lyras, A. D. Panagopoulos *et al.*, "Capacity statistics evaluation for next generation broadband MEO satellite systems," *IEEE Transactions on Aerospace and Electronic Systems*, vol. 53, no. 5, pp. 2344–2358, 2017.

[3] B. S. Mysore, E. Lagunas, S. Chatzinotas *et al.*, "Precoding for satellite communications: Why, how and what next?" *IEEE Communications Letters*, vol. 25, no. 8, pp. 2453–2457, 2021.

[4] V. N. Ha, D. H. N. Nguyen, J. C. M. Duncan *et al.*, "User-Centric Beam Selection and Precoding Design for Coordinated Multiple-Satellite Systems," in *2024 IEEE 35th International Symposium on Personal, Indoor and Mobile Radio Communications (PIMRC)*, 2024.

[5] G. Eappen, J. L. Gonzalez, V. Singh *et al.*, "Optimal Linear Precoding Under Realistic Satellite Communications Scenarios," *IEEE Open Journal of Vehicular Technology*, vol. 6, pp. 81–91, 2025.

[6] J. Krivochiza, J. C. M. Duncan, J. Querol *et al.*, "End-to-end precoding validation over a live GEO satellite forward link," *IEEE Access*, pp. 1–10, 2021.

[7] L. M. Marrero, J. Duncan, J. Querol *et al.*, "Differential phase compensation in over-the-air precoding test-bed for a multi-beam satellite," in *2022 IEEE Wireless Communications and Networking Conference (WCNC)*, 2022, pp. 1325–1330.

[8] K. U. Storek, R. T. Schwarz, and A. Knopp, "Multi-satellite multi-user MIMO precoding: Testbed and field trial," in *IEEE International Conference on Communications (ICC)*, June, 2020.

[9] M. Á. Vázquez, X. Artiga, and A. I. Pérez-Neira, "Closed-form Multicast Precoding for Satellite Flexible Payloads," in *European Signal Processing Conference*, vol. 2021-Augus, 2021, pp. 910–914.

[10] F. Vidal, H. Legay, and G. Goussetis, "Joint Power, Frequency and Precoding Optimisation in a Satellite SDMA Communication System," in *2020 10th Advanced Satellite Multimedia Systems Conference and the 16th Signal Processing for Space Communications Workshop, ASMS/SPSC 2020*, 2020.

[11] F. Vidal, H. Legay, G. Goussetis *et al.*, "A system approach to enable digital beamforming with direct radiating arrays: The joint use of precoding and sparse arrays," *International Journal of Satellite Communications and Networking*, vol. 39, no. 6, pp. 645–660, 2021.

[12] J. A. Vásquez-Peralvo, J. C. M. Duncan, R. Palisetty *et al.*, "Wide-Beamwidth Circular Polarized Antenna for Diversity Combining Applications," in *2022 IEEE Globecom Workshops (GC Wkshps)*, 2022.

[13] "CCSDS recommendations for radio frequency and modulation systems: Earth Stations and Spacecraft," 2021.

[14] L. M. Marrero, J. C. M. Duncan, J. L. González *et al.*, "Accurate Phase Synchronization for Precoding-Enabled GEO Multibeam Satellite Systems," *IEEE Open Journal of the Communications Society*, vol. 5, pp. 712–729, 2024.

[15] L. M. Marrero, A. Haqiqatnejad, J. C. M. Duncan *et al.*, "Multiuser-MISO Precoding under Channel Phase Uncertainty in Satellite Communication Systems," *IEEE Open Journal of Vehicular Technology*, vol. 4, pp. 127–148, 2023.

[16] J. Duncan, J. Krivochiza, S. Andrenacci *et al.*, "Hardware demonstration of precoded communications in multi-beam UHTS systems," in *36th International Communications Satellite Systems Conference (ICSSC 2018)*, 2018.

[17] J. L. González-Rios, L. Martínez-Marrero, E. Lagunas *et al.*, "Doppler Shift in Precoded Cooperative Multi-Gateway Satellite Systems: Effects and Mitigation," in *2024 IEEE Wireless Communications and Networking Conference (WCNC)*, 2024.

[18] J. L. González-Rios, E. Lagunas, H. Al-Hraishawi *et al.*, "In-Lab Carrier Aggregation Testbed for Satellite Communication Systems," in *30th Ka and Broadband Space Communications Conference*, 2025.

[19] R. Palisetty, L. M. G. Socarras, H. Chaker *et al.*, "FPGA Implementation of Efficient Beamformer for On-Board Processing in MEO Satellites," in *2023 IEEE 34th Annual International Symposium on Personal, Indoor and Mobile Radio Communications (PIMRC)*, 2023.

[20] L. M. Garcés-Socarrás, J. L. González-Rios, R. Palisetty *et al.*, "Efficient Digital Beamforming for Satellite Payloads Using a 2D FFT-Based Parallel Architecture," in *2025 IEEE International Symposium on Circuits and Systems (ISCAS)*, 2025.

[21] J. A. Vásquez-Peralvo, J. Querol, F. Ortíz *et al.*, "Flexible Beamforming for Direct Radiating Arrays in Satellite Communications," *IEEE Access*, vol. 11, pp. 79 684–79 696, 2023.

[22] ——, "Multibeam Beamforming for Direct Radiating Arrays in Satellite Communications Using Genetic Algorithm," *IEEE Open Journal of the Communications Society*, vol. 5, pp. 2343–2357, 2024.